# Cubic GaN and InGaN/GaN quantum wells ⓕ

ⓘD D. J. Binks, ⓘD P. Dawson, ⓘD R. A. Oliver, et al.

**COLLECTIONS**

ⓕ This paper was selected as Featured

View Online     Export Citation     CrossMark

## ARTICLES YOU MAY BE INTERESTED IN

Defect-characterized phase transition kinetics
Applied Physics Reviews **9**, 041311 (2022); https://doi.org/10.1063/5.0117234

Charge-transfer-enhanced d–d emission in antiferromagnetic NiPS₃
Applied Physics Reviews **9**, 041406 (2022); https://doi.org/10.1063/5.0107065

Wide bandgap semiconductor materials and devices
Journal of Applied Physics **131**, 230401 (2022); https://doi.org/10.1063/5.0100601

AIP Publishing

# Cubic GaN and InGaN/GaN quantum wells Ⓕ

D. J. Binks,[1] Ⓓ P. Dawson,[1] Ⓓ R. A. Oliver,[2,a] Ⓓ and D. J. Wallis[2,3,4] Ⓓ

### AFFILIATIONS

[1]Department of Physics and Astronomy and Photon Science Institute, University of Manchester, Manchester, United Kingdom
[2]Department of Materials and Metallurgy, University of Cambridge, Cambridge, United Kingdom
[3]Centre for High frequency Engineering, Cardiff University, Cardiff, United Kingdom
[4]Kubos Semiconductors, Ltd., Future Business Centre, Cambridge, United Kingdom

[a]Author to whom correspondence should be addressed: rao28@cam.ac.uk

### ABSTRACT

LEDs based on hexagonal InGaN/GaN quantum wells are dominant technology for many lighting applications. However, their luminous efficacy for green and amber emission and at high drive currents remains limited. Growing quantum wells instead in the cubic phase is a promising alternative because, compared to hexagonal GaN, it benefits from a reduced bandgap and is free of the strong polarization fields that can reduce the radiative recombination rate. Initial attempts to grow cubic GaN in the 1990s employed molecular beam epitaxy, but now, metal-organic chemical vapor deposition can also be used. Nonetheless, high phase purity requires careful attention to growth conditions and the quantification of any unwanted hexagonal phase. In contrast to hexagonal GaN, in which threading dislocations are key, at its current state of maturity, the most important extended structural defects in cubic GaN are stacking faults. These modify the optical properties of cubic GaN films and propagate into active layers. In quantum wells and electron blocking layers, segregation of alloying elements at stacking faults has been observed, leading to the formation of quantum wires and polarized emission. This observation forms part of a developing understanding of the optical properties of cubic InGaN quantum wells, which also offer shorter recombination lifetimes than their polar hexagonal counterparts. There is also growing expertise in p-doping, including dopant activation by annealing. Overall, cubic GaN has rapidly transitioned from an academic curiosity to a real prospect for application in devices, with the potential to offer specific performance advantages compared to polar hexagonal material.

## TABLE OF CONTENTS

## I. INTRODUCTION

Polar InGaN/GaN quantum wells (QWs), that is, QWs grown along the c-axis of the hexagonal wurtzite crystal phase, are the basis of LED technology that is enabling solid-state lighting to become dominant across many illumination applications.[1] These LEDs can have a luminous efficacy that exceeds that of all previous lighting technologies

while also being economically competitive and have resulted in significant reductions in overall energy usage with a consequently reduced environmental impact.[1] Nevertheless, important opportunities still exist to further improve device performance. In particular, improving the efficiency of InGaN/GaN QWs emitting in the green and amber part of the spectrum would enable further improvements in luminous efficacy by allowing white light to be efficiently generated by a combination of multi-colored LEDs, rather than relying on the downconversion of blue LED emission by a phosphor. Increasing luminous efficacy at high drive currents is also an important goal that will enable LEDs suitable for high brightness applications, such as vehicle headlights.

An important feature of the wurtzite phase grown along the c-axis is the large internal electric field that arises across QWs, which is a consequence of the polar nature of this hexagonal crystal structure. This internal electric field causes a redshift of the emission energy, known as the quantum confined stark effect (QCSE), and importantly also results in the spatial separation of electrons and holes in the QW, limiting their wave-function overlap and thus decreasing the rate of radiative recombination. This separation is exacerbated both for wider wells, which makes greater separations possible, and by greater indium content, which increases the strength of the internal field. Radiative recombination thereby becomes less competitive with non-radiative processes, significantly reducing the efficiency of the higher indium content QWs required for longer wavelength emission.[2] Furthermore, a reduced overall rate of recombination increases the carrier concentration in the QW produced by a given drive current, leading to an increased rate of carrier concentration-dependent non-radiative processes, such as Auger recombination and carrier delocalization followed by capture by defects.[3] The growth of the wurtzite phase along directions other than the c-axis has been explored to produce semipolar or non-polar QWs (i.e., with reduced or eliminated internal fields), but this has yet to have a significant impact on commercial devices.

One approach to overcome the limitations resulting from the presence of the internal electric field in InGaN/GaN QWs grown in the hexagonal phase is to produce them instead from crystals grown in the cubic phase. This has the zinc-blende structure,[4] as seen in more conventional compound semiconductors such as GaAs, and therefore, except under certain circumstances such as shear stress, the internal electric fields are completely removed. However, the zinc-blende phase of GaN is not thermodynamically stable under most growth conditions, and therefore, the production of high-quality films is challenging. Despite this, there is a body of scientific literature on the growth of cubic GaN that dates to the early 1990s, in which groups have reported the successful demonstration of the growth of films with at least some cubic phase content. However, due to the rapid performance enhancements that were made in devices in the wurtzite phase, the initial flurry in activity on cubic GaN died away in the early 2000s with only a small number of groups continuing work in this area. Currently, the continuing limitations to the efficiency of wurtzite InGaN/GaN LEDs under certain key conditions, particularly when emitting in the green and amber parts of the spectrum or at high drive currents, is motivating a renewed interest in the cubic phase.

This review will describe recent developments in cubic GaN: the latest growth techniques that have enabled the production of high-quality epilayers and QW structures; the importance of defects,

particularly stacking faults; and the emission properties of both epilayers and QWs. Finally, the outlook for this promising material will be discussed.

## II. A COMPARISON OF KEY PROPERTIES BETWEEN WURTZITE AND ZINC-BLENDE PHASES

In addition to the absence of the internal electric fields in QWs, the cubic phase has other properties, which make it of particular interest for light-emitting devices. As shown in Table I, cubic GaN has a bandgap that is 200 meV smaller than the wurtzite phase. A similar reduction in bandgap is also expected for InGaN alloys and, therefore, in order to achieve a given emission wavelength, less indium is required in a QW. This is important because the growth of high quality, high indium content QWs is particularly challenging in polar and non/semi-polar hexagonal structures. Thus, the reduced bandgap of cubic InGaN coupled with the lack of the internal field, which allows wider QWs to be grown without appreciably decreasing wave-function overlap, meaning that for a given emission wavelength, significantly less indium is required, and therefore, the constraints on the growth conditions are relaxed. As an example of this, we have demonstrated that for 10 nm thick 11% In QWs, we are able to achieve emission at 540 nm in cubic GaN MQW structures—see Fig. 1.

Another interesting property of cubic GaN is that calculations suggest that holes have a lower effective mass than in the hexagonal phase.[5] This would result in higher hole mobility, and there is some evidence in the literature that this is seen experimentally. An example of this is the work by Hernández-Gutiérrez *et al.* who have measured hole mobilities of $\approx 100 \, \text{cm}^2/\text{V s}$ at a hole concentration of $1 \times 10^{17} \, \text{cm}^{-3}$ in molecular beam epitaxy (MBE) grown cubic GaN.[6] Interestingly, they also measure a maximum hole concentration of $6 \times 10^{19} \, \text{cm}^{-3}$, which is significantly higher than that seen in hexagonal GaN and suggesting that the activation of Mg may be more efficient in the cubic phase. One of the key contributing factors to efficiency droop in polar LEDs is the inability to supply sufficient holes to the QWs at high current densities. Thus, the ability to produce higher hole concentrations with greater mobility would significantly mitigate this issue.

In summary, the removal of the internal electric fields, reduced bandgap, and higher hole mobility and concentrations all make the cubic phase of GaN an interesting system to further improve the performance of GaN based LEDs.

**TABLE I.** Comparison of key parameters for hexagonal and cubic GaN.

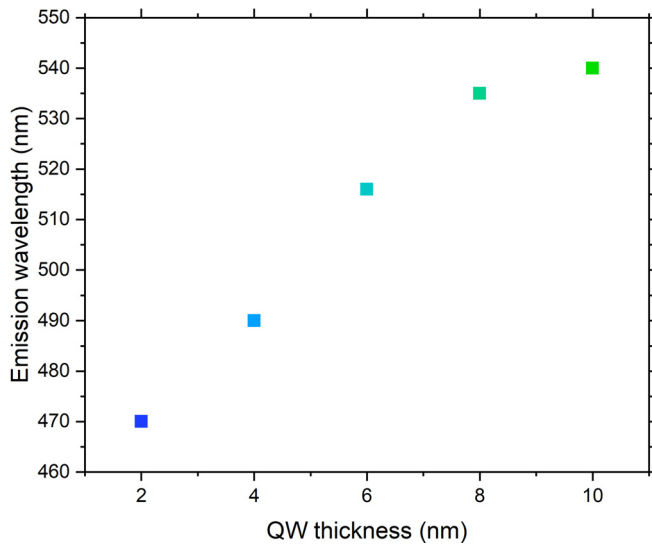| Property | Hexagonal GaN | Cubic GaN |
|---|---|---|
| Internal electric fields | Yes | No |
| Bandgap (300 K) | 3.4 eV (Ref. 7) | 3.2 eV (Ref. 7) |
| Electron mobility (at 300 K and $1 \times 10^{17} \, \text{cm}^{-3}$ carrier concentration) | 600 cm$^2$/V s (Ref. 8) | 1800 cm$^2$/V s (Ref. 9) |
| Hole mobility (at 300 k and $1 \times 10^{17} \, \text{cm}^{-3}$ carrier concentration) | 40 cm$^2$/V s (Ref. 10) | 100 cm$^2$/V s (Ref. 6) |
| Maximum free hole concentration | $3 \times 10^{18} \, \text{cm}^{-3}$ (Ref. 10) | $6 \times 10^{19} \, \text{cm}^{-3}$ (Ref. 6) |

FIG. 1. Peak photoluminescence (PL) emission wavelengths for InGaN QWs with approx. 11% indium and widths between 2 and 10 nm.
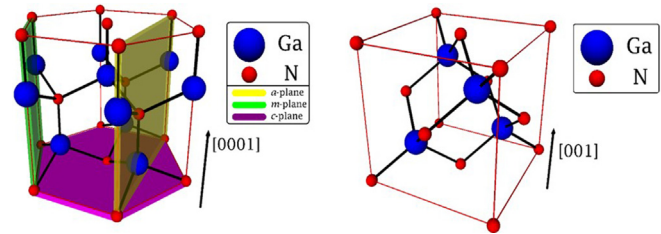


FIG. 2. Crystal structures of hexagonal (left) and cubic (right) GaN. For hexagonal GaN, growth is most common in the direction normal to the c-plane but is also possible in alternative directions, such as normal to the a- and m-planes, both of which are shown here. For cubic GaN, growth is normally performed on the (001) plane.

## III. GROWTH

Two growth techniques are commonly used for the growth of high-quality semiconductor thin films. These are molecular beam epitaxy (MBE) and metal organic chemical vapor deposition (MOCVD), also known as metal organic vapor phase epitaxy (MOVPE). MBE is an ultra-high vacuum (UHV) growth technique, and the crystal growth process is often controlled by kinetic, rather than thermodynamic effects. For this reason, in principle, MBE offers more opportunities to force the growth of non-equilibrium phases. However, MOCVD is easily scalable to multi-wafer systems to give low cost per wafer and, therefore, is the dominant growth platform for the commercial production of semiconductor devices and, in particular, hexagonal GaN for LEDs and high electron mobility transistors. Thus, both techniques have been used for the growth of cubic GaN. The choice of the substrate is an important consideration for both MBE and MOCVD growth, so this is also discussed below.

### A. Substrates

The crystal structures of the hexagonal and cubic phases of GaN are shown in Fig. 2. The two phases are very closely related, maintaining tetrahedral bonding of the gallium and nitrogen atoms and with only the stacking sequences of the atomic planes differing. Considering (as an example) the Ga sublattice, in zinc-blende, the stacking sequence along the $\langle 111 \rangle$ directions may be written as –ABCABC-, whereas the wurtzite stacking sequence along the equivalent $\langle 0001 \rangle$ direction is –ABAB-. As a consequence of this similarity in the structure, the difference in the formation energy of different phases is relatively small on the order of 10 meV.[11] In the absence of bulk cubic GaN crystals, the choice of a suitable substrate is critical for the high-quality growth of the cubic phase. Typically, a substrate is chosen, which provides a zinc-blende template that should help to stabilize the cubic phase. In the literature, several substrates for cubic GaN growth have been trialed. These include GaAs,[12,13] silicon,[14,15] silicon with the surface carbonized to give a very thin layer of 3C-SiC,[16] bulk 3C-SiC,[17] and thick layers of 3C-SiC deposited epitaxially on Si.[18] Since the predominant orientation for these substrates is [001], this is the most common orientation that is used for the growth of cubic GaN, although there are some examples of [111] oriented substrates being used.[19] While varying degrees of success have been seen on various substrates trialed, all have challenges.

The first of these challenges is the lattice mismatch to cubic GaN. As seen in Table II, GaAs and Si have relatively large lattice mismatches to cubic GaN and, thus, introduce a very high number of defects into the epitaxial nucleation layer. It is possible that this limits the phase purity of the epitaxy as the defects could act as nucleation sites for the hexagonal phase. 3C-SiC has a relatively small lattice mismatch to cubic GaN, variously reported as being from 3.4%[20] to 3.7%.[7] However, this would still give a critical thickness for relaxation of only a few monolayers, and therefore, the nucleation of the film must be carefully controlled.

A second challenge for growth on dissimilar substrates is the difference in thermal expansion coefficient between the film and the substrate. Since the films are usually grown at relatively high temperatures (i.e., >700 °C) as the layer is cooled to room temperature, a difference in the thermal expansion will also cause strain in the layers and hence bowing of the substrate similar to that seen for conventional GaN layers.[21] If the strain introduced in the epilayer is tensile, as is the case for cubic GaN on Si, this can result in cracking of the film, which is catastrophic for device layers. However, even for relatively small strains, the resultant bowing of the substrate can be problematic as the change in height across the wafer causes issues when photolithography is used to manufacture devices. Typically, the limit of a wafer bow that still allows commercial high yield manufacturing is 50 $\mu$m for a 150 mm wafer, and therefore, methods must be found to control the strain due to thermal expansion differences. As seen in Table II, the thermal expansion mismatch is relatively small for GaAs substrates but is significant for SiC and Si substrates; however, to date, we are not aware of any published work in cubic GaN to manage the thermal expansion mismatch to the growth substrates. Inspired by strategies used to manage thermal mismatch in hexagonal GaN growth on Si,[21] however, our preliminary experiments suggest that it is possible to trap strain in cubic GaN layers which can counteract the thermal expansion mismatch.

A final challenge for the growth of (001) oriented films onto Si substrates is different step structures that are possible on Si compared to a compound semiconductor. As illustrated in Fig. 3(a), when the Si

**TABLE II.** Lattice parameters and thermal expansion coefficients of common growth substrates, with associated mismatches to cubic GaN. All data from Ref. 7.

| Substrate | Lattice parameter | Lattice parameter mismatch to cubic GaN | Coefficient of thermal expansion | Coefficient of thermal expansion mismatch to cubic GaN |
|---|---|---|---|---|
| Cubic GaN | 0.452 nm | 0% | $\approx 5.6 \times 10^{-6}\,K^{-1}$ | 0% |
| GaAs | 0.5653 nm | −20.0% | $5.7 \times 10^{-6}\,K^{-1}$ | −1.7% |
| Silicon | 0.5431 nm | −16.8% | $2.6 \times 10^{-6}\,K^{-1}$ | +115% |
| 3C-SiC | 0.4360 nm | +3.7% | $2.8 \times 10^{-6}\,K^{-1}$ | +100% |

unit cell is terminated, the surface can have steps that are a 1/4-unit cell in height. Due to a different bonding at these steps, the symmetry of the crystal is rotated by 90° and, thus, when the cubic GaN (or any other III-V material) is nucleated, domains of crystal with different orientations result. This gives rise to anti-phase domain defects in the GaN film as seen in Fig. 3(c).[22] Such issues can be overcome by using off-cut substrates and careful annealing of the Si substrate surface to force only double-height steps, as shown in Fig. 3(b), to exist. However, the very limited growth window for cubic GaN growth means that this is likely to be difficult to achieve for growth directly onto Si. The use of intermediate layers such as 3C-SiC in conjunction with substrate off-cut does, however, allow single domain cubic GaN layers to be produced as seen in Fig. 3(d). The use of intermediate layers of graphene has also allowed single domain films to be demonstrated.[23]

Another approach that has been demonstrated to stabilize the cubic phase of GaN is growth into V-grooves patterned onto Si (001) substrates. In the V-grooves, the (111) facets of the Si crystal are exposed and onto these hexagonal GaN is nucleated with the hexagonal ⟨0001⟩ planes parallel to the Si ⟨111⟩ planes, as shown in Fig. 4. As the hexagonal phase grows from the (111) and (−1–11) facets where the two growth fronts meet the cubic phase has been shown to form. Stark *et al.*[14] have used this technique to demonstrate micrometer-scale green LEDs on large-area Si wafers with the potential to scale up to 300 mm wafers. However, outside the grooves the hexagonal phase dominates, and so significant challenges exist in taking this to volume production for large area LEDs.

## B. MBE

As described above, MBE is a UHV technique in which an elemental beam of atoms or molecules impinges on a substrate surface. Since the substrate surface is not populated by atoms or molecules from the ambient atmosphere, the diffusion length of adatoms tends to be dominated by the surface kinetics and, thus, the substrate temperature. In many ways, this is ideal for cubic GaN as it offers the
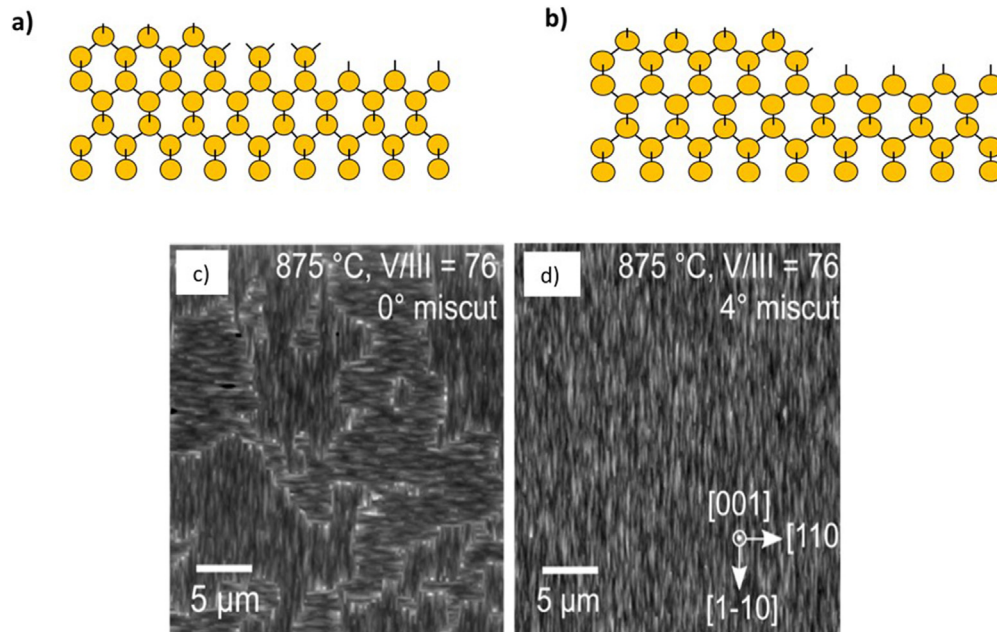


**FIG. 3.** Schematic of (a) single and (b) double height surface steps in silicon. (c) shows an atomic force microscopy image (AFM) of the surface of a cubic GaN layer grown onto 0° miscut (SiC)/Si substrate with multiple anti-phase domains due to single-height Si surface steps. (d) shows AFM of a similar cubic GaN layer grown on a 4° miscut (SiC)/Si substrate where the anti-phase domains are removed. Parts (c) and (d) are reproduced with permission from J. Appl. Phys. **124**, 105302 (2018). Copyright 2018 AIP Publishing.

**FIG. 4.** Growth of cubic-GaN from V-grooves on Si. Reproduced with permission from Appl. Phys. Lett. **103**, 232107 (2013). Copyright 2013 AIP Publishing.
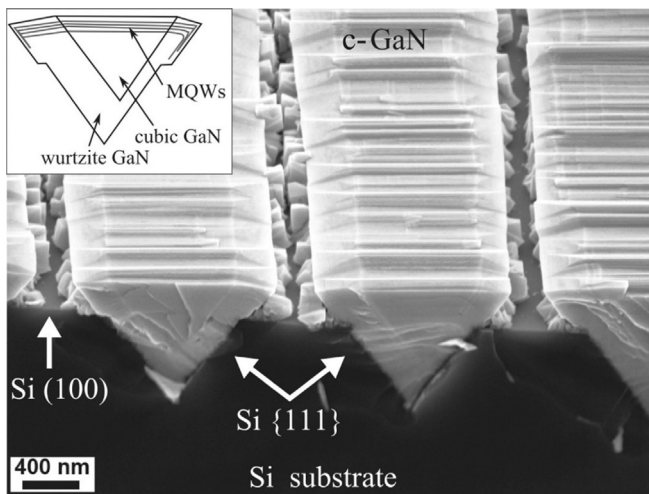
opportunity to force the growth away from the thermodynamically stable phase and "trap" the structure in the cubic phase. Thus, initial attempts to grow the cubic phase of GaN in the early 1990s were dominated by the MBE technique.

The group III sources used for the MBE growth of GaN is metallic gallium. For the nitrogen source, the most common option is $N_2$. However, as $N_2$ is not easily dissociated by pyrolysis, an $N_2$ plasma source must be used to generate nitrogen radicals. The technique of plasma-assisted MBE is the most common method that has been applied to the growth of cubic GaN over the years. In principle, $NH_3$ can be used as a nitrogen source in MBE and has advantages as it can be cracked at much lower temperatures than $N_2$, and therefore, a plasma source is not required. A $NH_3$ source MBE has been used for hexagonal GaN growth.[24] However, $NH_3$ brings additional challenges as it can condense onto the cryo panels used to give high levels of vacuum in MBE systems and also releases H atoms, which modify the surface energy of the crystal as it is growing. Hydrogen can also form complexes with dopant atoms, which impact dopant activation.[25] We are not aware of any attempts to grow cubic GaN using $NH_3$ as a nitrogen source in MBE.

Clearly, the nucleation stage of the growth is critical to achieving high-quality cubic GaN layers irrespective of the substrate. For MBE growth on GaAs, the substrate surface is usually prepared by growing a GaAs buffer layer. In the case of growth on Si, the surface is usually prepared by first removing the native oxide at high temperature and then converting the Si surface to silicon carbide by exposure to a hydrocarbon, for example, $C_2H_2$ at 970 °C.[26] Growth of the film is then typically initiated by the growth of a nucleation layer at temperatures in the range 588[27]–620 °C[28] with a thickness of a few monolayers irrespective of the substrate. Yang *et al.* study the effect of the V/III ratio during the nucleation layer on the structural properties of the film and show that a V/III ratio close to stoichiometric composition is important to give high-quality cubic GaN layers.[28] This is reinforced by other studies who also find that in MBE V/III ratios close to unity or very slightly Ga-rich give the best quality films. For the growth of

the main cubic GaN layer, the growth temperature is usually raised to between 650[27] and 750 °C.[29] The work by Jenkins *et al.*[30] and Novikov *et al.*[31] has also suggested that, at least for growth on GaAs, the presence of low levels of As in the nucleation layers may also help to stabilize the cubic phase.

### C. MOCVD

MOCVD is by far the dominant growth technology for commercial production of GaN-based LEDs and electronic devices. Therefore, for a device technology based on cubic GaN to be commercially competitive in anything but the smallest niche applications, it is likely that it will need to be compatible with MOCVD growth. However, the growth of GaN by MOCVD typically requires higher temperatures than MBE, and therefore, the window for the successful growth of the cubic phase is likely to be smaller than that for MBE. Despite this, the earliest example of cubic GaN growth that we can find is actually by MOCVD.[32] However, since MOCVD is a relatively high-pressure technique, an important additional consideration is the control of non-intentional impurities such as oxygen and carbon, which is known from MOCVD growth of hexagonal GaN to be challenging. The narrower window of growth conditions required for cubic GaN is likely to be exacerbate this issue. There are only limited studies in the literature addressing this question. For the case of oxygen, this implies that sufficiently leak-free reactor designs must be used, although this is not a significant issue for well-maintained modern commercial MOCVD reactors. Control of carbon, however, could be more challenging as this is present in the metal-organic precursors used for MOCVD growth and it is known that carbon incorporation is enhanced at the low V/III ratios[33] and (based on understanding from hexagonal growth) the low temperatures[34] used in cubic GaN. The impacts of carbon on the optical properties of cubic GaN are discussed in Sec. V.

As for MBE, a key step in the MOCVD growth process is the nucleation of the GaN layer onto the dissimilar substrates typically used. It was found during the very early work on MOCVD growth of hexagonal GaN on sapphire that the key to achieving high-quality films was the use of a two-step growth process.[34] This involves nucleation of the film at low temperature to ensure a high density of nucleation sites followed by an annealing step and then growth at higher temperature to give a high-quality coalesced film. Most work on cubic GaN using MOCVD has followed a similar approach with a low-temperature nucleation step in the range 550–650 °C[35] followed by higher temperature growth of the remainder of the layer. This nucleation layer typically has a thickness between 20[36] and 60 nm.[17] Growth is then paused and the temperature raised to the growth temperature of the final layer providing the annealing step. Notable differences in the MOCVD growth of cubic-GaN layers is that the growth of hexagonal GaN is normally carried out at a high temperature, i.e., >1000 °C, and a high V-III ratio (>1000:1) in order to ensure high-quality films. However, a review of the literature[18,37,38] and our growth experiments[22] show that high-quality cubic phase films are only possible at relatively low temperatures, i.e., <900 °C and V-III ratios (<500:1). The precise growth conditions to give the highest quality c-GaN films are still being investigated, so it is not possible at this time to definitively describe how the growth process should be optimized, although good progress toward device quality films has been made.

## IV. DEFECTS

### A. Phase purity

Due to the small difference in the formation of energy between the cubic and hexagonal phases of GaN, one of the key challenges in producing high-quality cubic GaN layers is the prevention of the spontaneous nucleation of the hexagonal phase. This is likely to happen at defects on the surface of the growing layer, and particularly, if $(111)_{ZB}$ facets become exposed due to surface roughening. This is because the cubic and hexagonal phases differ only in their stacking sequence along the $[111]_{ZB}/[001]_{WZ}$ directions, and therefore, the energy difference is only due to weak second neighbor interactions. In order to judge the quality of cubic GaN layers, techniques are required, which can differentiate between the two phases and ideally give a quantitative measure of the relative propositions of the two phases. While, in principle, there are several characterization techniques that can measure the relative proportion of the phases of a layer, care must be taken to understand the limitations of various techniques to ensure that an accurate assessment of the film quality is given. This is an area that is often neglected in the literature and, therefore, some of the claims made about film "quality" are vague and difficult to interpret. Hence, we will now discuss each of the main techniques in turn.

#### 1. Optical spectroscopy

As shown in Table I the room temperature bandgap of cubic and hexagonal GaN differ by approximately 200 meV. Thus, the near band edge (NBE) photoluminescence (PL) can provide a signature that differentiates between the two phases as seen in Fig. 5, which shows the room temperature near band edge PL spectra for phase pure zincblende and wurtzite GaN films.

In practice, however, the details of the PL emission depend on several factors, which can modify the spectra and give rise to misleading results, particularly, if the film is an intimate mixture of the two GaN phases. First, the position of the near band edge PL can be
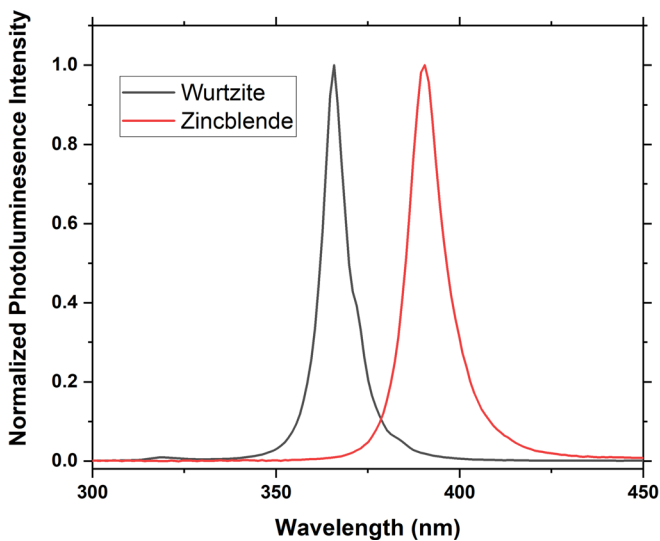


**FIG. 5.** Room-temperature PL spectra for phase pure cubic and hexagonal GaN layers showing the shift in band edge emission energy.

modified by strain. Due to the slightly different lattice constants of the two phases, it is likely that for a film that consists of an intimate mixture of phases, there will be strain, which will cause a small variation in the precise position of the near band edge peaks around their ideal energy. However, for typical values of strain expected, the peak shifts are relatively small compared to the difference due to the bandgap difference, and therefore, this is not a significant issue for differentiating between the phases. A second issue, which plays a much more significant role, is carrier diffusion within the layer. Due to the finite lifetime of the carriers in the sample, before they recombine to emit light, they have the opportunity to diffuse within the layer. Due to the narrower bandgap of the cubic phase, carriers will tend to diffuse out of the hexagonal phase, and therefore, the intensity of the associated NBE peak can be significantly reduced. The diffusion length in high-quality hexagonal GaN is of the order of 100 nm,[39] and therefore, any inclusions smaller than about 200 nm in extent are likely to give a very low intensity near band edge signal. A third point is that all the PL emission processes are the results of competition among various emission channels. This implies that impurities, defects, and free surfaces, which may all cause non-radiative recombination, may also have an impact on the NBE emission intensity. For the above bandgap excitation, the extinction depth of the pump laser is of the order of 100 nm,[40] and therefore, surfaces may play a major role in determining the PL signal. From our experiments, we see that it is possible to have layers with up to 30% hexagonal phase (measured by x-ray diffraction), which show no evidence of hexagonal band edge emission in room temperature PL.

In many ways, the use of Raman spectroscopy is more sophisticated than PL in that the vibrational modes of interest, namely, the cubic longitudinal optical (LO) mode and the hexagonal A1(LO) have very similar energy, namely, 740 and 735 cm$^{-1}$ but polarization selection can be used to discriminate between them. This subject has been extensively discussed by Haboeck $et~al.$[41]

#### 2. X-ray diffraction

X-ray diffraction is probably the most common characterization technique used to examine the quality of cubic GaN films and a comprehensive review of x-ray diffraction techniques in cubic-GaN is given by Frentrup $et~al.$[20] The key points are

(1) Appropriate reflections must be chosen that have sufficient separation in $2\theta$ between the cubic and hexagonal phases.

(2) The extinction depth of x-rays is of the order of several micrometers, and therefore, x-ray measurements give a surface weighted average of the whole film thickness. This means that x-ray diffraction should only be used to compare samples with similar thickness, and as the phase purity of a layer will often evolve with film thickness extreme, care must be used in interpreting results. Often a variety of techniques are required to give a comprehensive view of the microstructure of a film.

(3) The contribution of defective regions of the film to the x-ray intensity must be carefully considered. A high density of stacking faults within a pure cubic GaN layer will give rise to streaks of intensity in reciprocal space. These can result in significant diffracted intensity at the position of diffraction peaks from hexagonal GaN. Therefore, care must be taken to differentiate between intensity from hexagonal material and defective cubic GaN.
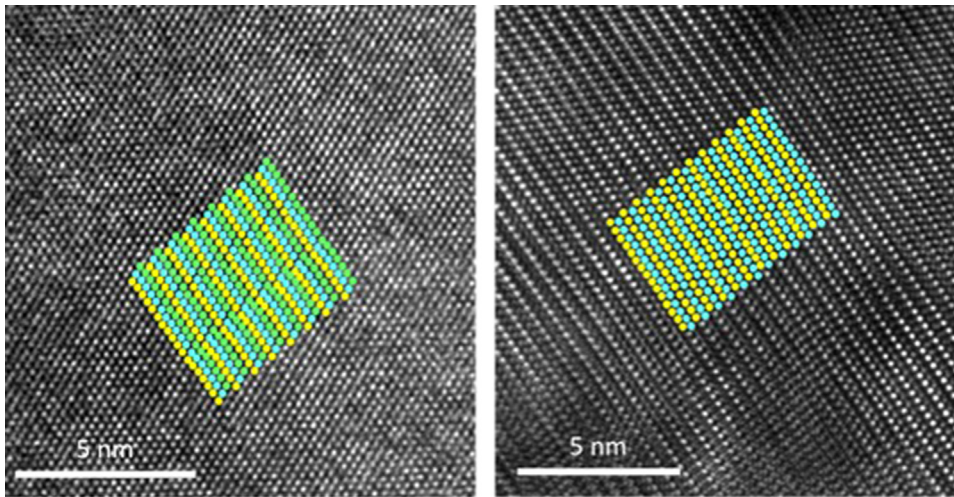
**FIG. 6.** High resolution scanning transmission electron microscopy (HRSTEM) images of (a) cubic GaN stacking and (b) hexagonal GaN stacking. In (a), the yellow, blue, and green dots illustrate the -ABCABC- stacking, whereas in (b), the yellow and blue dots illustrate the –ABAB-stacking.

### 3. Transmission electron microscopy

Transmission electron microscopy (TEM) allows the direct study of a film's microstructure. It is, therefore, possible to directly image the crystal structure of a layer. This is illustrated in Fig. 6, which shows lattice resolution images of (a) cubic and (b) hexagonal regions of a film where the stacking sequence of the two phases can be clearly differentiated. To study a wider area, it is possible to use scanning electron diffraction (SED), which involves the rastering of the electron beam across the sample surface and the acquisition of an electron diffraction pattern at each probe position. Theoretical diffraction patterns may be simulated, and automated pattern matching across the area scanned is then used to produce a map of the phases present in the sample,[42] as shown in Fig. 7. TEM also gives information about the defect distribution and structure in the film and structure at the substrate-to-layer interface. Thus, TEM is one of the most powerful techniques for the characterization of the quality of cubic GaN films. One of the key limitations of TEM techniques is the very small volume of material that can be inspected, so care must be taken that any conclusions that are drawn for a particular TEM sample are representative of the whole of the sample.
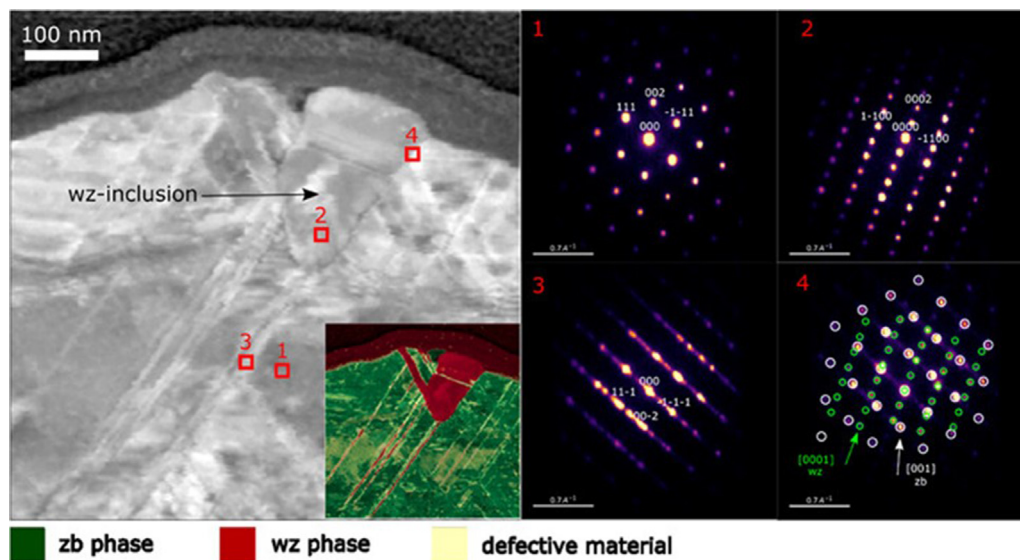


**FIG. 7.** Illustration of scanning electron diffraction mapping of a cubic GaN film containing a hexagonal inclusion. The main image on the left is a virtual bright-field (BF) scanning electron diffraction (SED) image. Diffraction patterns taken from four labeled regions are shown on the right. Region 1 is in the main body of the cubic GaN film. Region 2 is on a hexagonal inclusion. Region 3 is a stacking fault bunch, and region (4) is at the boundary between the hexagonal and cubic material. The inset of the virtual BF image is the phase map obtained by SED imaging, where the cubic phase is highlighted in green, while the hexagonal phase is marked in red and defective material is marked in yellow. Reproduced with permission from J. Appl. Phys. **130**, 115705 (2021). Copyright 2021 AIP Publishing.

## B. Stacking faults

Stacking faults (SFs) can be present in both the hexagonal and cubic phases of GaN and several studies of the properties of stacking faults in hexagonal GaN,[43,44] including those which occur in nanowires,[45,46] exist. However, the properties of SFs in cubic GaN are much less well understood. A key point to note is that an SF in cubic GaN is a region with hexagonal layer stacking. Given the lower formation energy of hexagonal GaN than cubic GaN, this means SFs must be expected to be a very common defect in the cubic material. Additionally, the SF is a thin region of wide bandgap material in a low bandgap matrix. This contrasts with a SF in hexagonal GaN, which is a region of low bandgap material in a wideband gap matrix, so the electrical and optical properties are likely to be very different. Calculations for SFs in hexagonal GaN suggest that the SF and bulk have type-II band alignment where the conduction band of the SF is higher than that of the surrounding hexagonal matrix.[47] This type-II band alignment is likely to also be present for SFs in cubic GaN, but to date, studies of the properties of SFs in cubic GaN are very limited.

Recently, a specific broad recombination band associated with the presence of SFs in cubic GaN has been identified in low-temperature PL measurements.[48] This so-called high energy band (HEB) was observed at around 3.4 eV, i.e., between the low-temperature bandgaps of cubic GaN (3.3 eV) and hexagonal GaN (3.5 eV). Apart from the spectral position and the width of the feature, it was noted that the recombination lifetime at low temperatures varied between 0.15 and 0.67 ns with decreasing detection energy. These observations were explained by considering pairs of SFs to be quantum barriers that confine carriers in the cubic GaN region between them, thus forming a QW, as illustrated in Fig. 8; the distance between SF pairs varies resulting in a range in the degree of quantum confinement. As the spontaneous polarization of the hexagonal GaN is different from the cubic GaN, then electric fields may exist in both phases of GaN, although recent calculations indicate that the magnitudes of
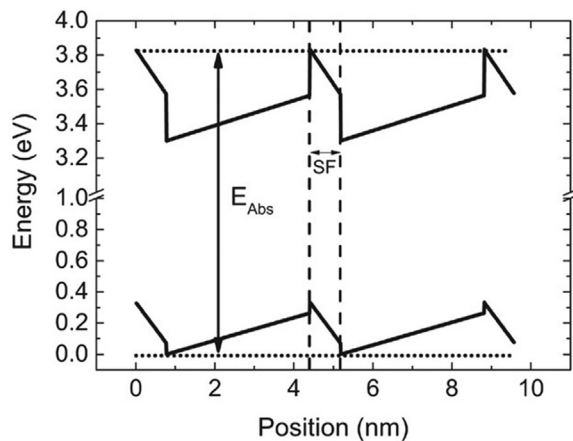
these fields on the nanoscale are weaker than expected from considering only bulk polarization properties.[49] By solving Schrödinger's equation for a range of SF separation the range of resultant recombination energies is compatible with the width of the HEB. Furthermore, the range of recombination times is qualitatively compatible with the range of electron–hole wave function overlap that occurs in the SF cluster with varying separations.

SFs formed on the basal plane of hexagonal GaN in the c-plane orientation do not propagate into the active device layers. This is not true for non- and semi-polar orientations of the hexagonal crystal where any basal plane SFs generated during growth will penetrate into the active region. Since SFs degrade the optical properties of hexagonal GaN devices, there has been a significant research effort to understand how SF densities can be decreased. In most instances, this requires epitaxial lateral overgrowth onto patterned substrates.[50] For cubic GaN layers, the situation is slightly different since SFs occur on each of the four sets of ⟨111⟩ planes. This means that as the layer thickness increases SFs on intersecting (111) planes can meet and annihilate, which can lead to a significant reduction in SF density with film thickness.[51]

## C. Dislocations

Due to different symmetries of the cubic and hexagonal phases of GaN, the nature of the dislocations present in films is very different. In fact, since the crystal symmetry of cubic GaN is more similar to that of conventional semiconductors such as GaAs, dislocation types and dynamics will be closely related to these materials. For semiconductors such as GaAs, the 60° dislocation as illustrated in Fig. 9 is the dominant dislocation type. In cubic GaN, we have seen evidence for the formation of 60° dislocations at the layer substrate interface; however, the majority of them are dissociated into partial 30° and 90° dislocations, which bound SFs.[55] There is a large body of work on different types of dislocations possible in zinc blende semiconductors and how these dislocations interact. However, the subtleties of dislocations in cubic GaN have not been studied in any great detail as to date the high density of stacking faults has tended to dominate the layer properties. Clearly, as the quality of cubic GaN epilayers is improved and dislocations



**FIG. 8.** Band alignment in the region of a stacking fault in cubic GaN. The valence and conduction band offsets are taken to be 70 and 270 meV,[52] respectively, and the spontaneous polarization to be $-0.034\,cm^{-2}$.[53] The electric fields were calculated using the method due to Bernardini and Fiorentini.[54] Reproduced with permission from Church et al., Phys. Status Solidi B **254**, 1600733 (2017). Copyright 2017 John Wiley and Sons.
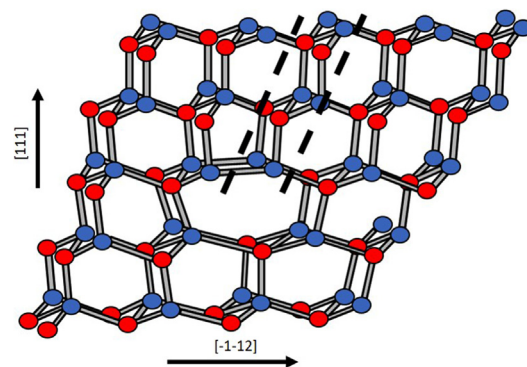


**FIG. 9.** Schematic of a 60° dislocation in the zinc-blende crystal structure. The additional plane of atoms is highlighted between the dashed lines. The blue circles represent the group III atomic sites, i.e., Ga and red circles represent the group V sites, i.e., N or As.

become the dominant defect, further work will be needed to understand the role of dislocations in determining layer properties.

## V. OPTICAL PROPERTIES

### A. Epilayers

Optical spectroscopies are useful tools for understanding carrier energetics and dynamics within epilayers, enabling key insights into the recombination process and the interaction of carriers with microstructural defects and impurities. Studying how PL spectra change with temperature and excitation power density provides information on, for example, exciton localization and binding energies and dopant activation energy, the identification of the type of state [such as free exciton, free carrier, donor-, or acceptor-bound or donor–acceptor pair (DAP)] involved in recombination, and defect and impurity density. In 2005, Reskikov and Morkoç[56] comprehensively reviewed the work on defect luminescence in both hexagonal and cubic GaN epilayers carried out up to that time. Furthermore, time-resolved PL (TRPL) allows the timescale of these processes to be determined, and how the rate of recombination is affected by the interactions of the carriers with defects and impurities. The related technique of PL excitation spectroscopy can aid in the identification of relaxation and recombination pathways, while photoreflectance (PR) spectroscopy and ellipsometry provide information on excitonic states.

When comparing reports of the energies of various types of optical transitions in epitaxial cubic GaN, it is worth noting that there will be an inevitable variation in the exact peak energies quoted by various authors as these energies will depend, among other things, on the strain state, which modifies the bandgap of the GaN. Before discussing the transitions seen in emission spectra, it should be taken into account that the fundamental optical process in semiconductors is the absorption of light and that the bandgap or more often the lowest lying free exciton peak is the best way to determine whether the strain plays a role in determining the PL emission energies. Absorption spectroscopy is the ideal technique to conduct this type of measurement but is a difficult technique to use, mainly because of the necessity of removing the substrate. Alternatively, PR spectroscopy can be used[57,58] to find the intrinsic free exciton transitions and thereby both measure the bandgap and determine the nature of the emission process(es). An example of this is provided in the work of Feneberg et al.[57] where temperature dependent PR spectra were recorded on a strain-free cubic GaN layer grown by plasma-assisted molecular beam epitaxy on a 3C-SiC(001) substrate. The PR spectra revealed two exciton transitions involving the degenerate heavy and light hole valence bands and the split off valence band. The lowest energy transition in PR at 5 K was at an energy of 3.271 eV, whereas the lowest energy PL transition at the same temperature was at 3.261 eV. The 10 meV energy difference, as confirmed by temperature dependent measurements, was ascribed to the binding energy of excitons at neutral donors. In comparison, Xu et al.[59] used PL to determine the free exciton recombination energy and reported a value of 3.268 eV at 10 K from a cubic GaN grown on GaAs by MOCVD.

Other optical transitions that are commonly observed in GaN epilayers involve bound excitons, donor-to-acceptor pairs (DAP), and deep impurity transitions. The relative strengths of these transition types in any spectra quite often reflect the density of a particular type of impurity or defect. However, this is not always the case, as the relative contributions to the spectra from different emission processes can

be modified by the excitation power density if saturable transitions are present. At low temperatures ($<30$ K), the excitonic transition typically seen in emission involves an exciton that is donor bound. For example, Yaguchi et al.[60] reported spectra measured at 5 K dominated by a bound exciton transition at 3.259 eV with a full width at half maximum height (FWHM) of 5 meV. This was obtained in a micro-PL measurement on the horizontal flat facet of a cubic GaN grain grown by MOCVD on 3C-SiC. Donor bound exciton recombination was also reported by Wu et al.[36] at 3.274 eV from MOCVD grown GaN on a GaAs substrate with a somewhat greater FWHM of 15 meV. In contrast, the bound exciton recombination from cubic GaN grown on GaAs by plasma-assisted MBE is reported to have a peak energy of 3.263 eV.[61] Other authors have reported similar values for the recombination energy of donor-bound excitons, including 3.279,[62] 3.263,[63] and 3.26 eV.[64]

At low temperatures, the DAP emission usually dominates over any transition involving a free carrier and either a neutral donor or acceptor, although this may depend on the degree of saturation of the DAP band and the concentration of donors and acceptors. The recombination energy $h\nu$ involving neutral donors and acceptors separated by a distance $r$ is given by

$$h\nu = E_g - E_D - E_A + \frac{e^2}{4\pi\varepsilon r^2}, \qquad (1)$$

where $E_g$ is the bandgap, $E_D$ is the donor ionization energy, $E_A$ is the acceptor ionization energy, $e$ is the electronic charge, and $\varepsilon$ is the dielectric constant. The last term on the right-hand side of the equation reflects the Coulomb interaction of the donor and acceptor states after recombination. The conventional signatures of DAP emission are a shift to higher energy with increasing excitation density due to the saturation of the low energy distant pair (i.e., large $r$) recombination and/or a decrease in the radiative lifetime with decreasing detection energy due to the decreased electron/hole wave-function overlap of the distant pairs. Note the peak emission energies can vary due to strain state but also due to excitation density, which causes a variation in the size of the Coulomb term. In general, the chemical identity of the donors and acceptors can play a significant role in the donor/acceptor recombination energies. Example reports include As et al.[64] who reported on the effects of unintentional and intentional doping on the energy of the DAP band in cubic GaN grown on GaAs. In unintentionally doped material, a DAP band is observed with a peak energy of 3.15 eV at 10 K with temperature-dependent measurements revealing the values of 25 and 130 meV for $E_D$ and $E_A$, respectively. As summarized by Reskikov and Morkoç,[56] there have been numerous other works reporting a similar peak energy for this transition;[61,63,65,66] up to two phonon replicas of this peak have also been reported, redshifted by 86 meV for the first replica and twice that for the second.[65] DAP emission at 3.08 eV has been associated with a deeper donor[63] and at 2.926 and 2.821 eV with deeper acceptors.[56]

A number of works have studied the spectral features produced or modified by doping. When cubic GaN is doped with carbon, a narrow peak at 3.08 eV made up of spectrally overlapping DAP recombination and electron-to-acceptor recombination processes was observed, which increased in intensity with the level of carbon doping.[67,68] Carbon doping also produces a broad yellow luminescence (YL) band, which also increases steadily with the carbon concentration.[67] As discussed in Sec. VI, doping with magnesium is commonly

used to produce the p-doped material in hexagonal GaN, which has motivated its study in cubic GaN. Mg-doping produces a broad blue luminescence (BL) band in cubic GaN centered around 2.9 eV,[69–73] and in some cases, a narrow and weak ultraviolet luminescence (UVL) band at around 3.05 eV.[72] Thermal annealing, which is used to reduce the concentration of Mg-H complexes and, thus, enhance the active p-doping, is observed to increase the intensity of the BB but reduces that of the UVL.[72] As it is for hexagonal GaN, doping with silicon is commonly used to produce n-type cubic GaN and has been observed to result in a redshift and broadening of the excitonic PL peak at about 3.26 eV, but a blueshift of the DAP peak at about 3.15 eV.[74]

An example of the PL spectra that result from these various recombination processes is shown in Fig. 10, which compares the PL spectra obtained at low temperature for an epilayer of high purity (>95%) cubic GaN to that for samples of hexagonal GaN and mixed cubic/hexagonal phase; all samples have been grown by MOCVD, with the cubic and mixed cubic/hexagonal GaN epilayers grown onto 3C-SiC and the pure hexagonal GaN deposited onto sapphire, respectively.

For the hexagonal GaN sample, a strong and narrow excitonic feature is seen at 3.48 eV, corresponding to the bandgap at this temperature; two phonon replicas, much weaker than the main feature, are also observed redshifted relative to the excitonic peak. Also, visible is the broad BL and YL bands associated with impurities. In contrast, the PL spectra for the high-phase purity cubic GaN sample consist of several overlapping peaks between 3.0 and 3.3 eV, varying the temperature and excitation power density allows the highest energy of these features to be identified as a donor-bound exciton and the others to be attributed to DAP recombination.[56] The energies of these near band edge features are consistent with a bandgap of 3.27 eV. The YL band is also visible, redshifted by the bandgap difference between hexagonal
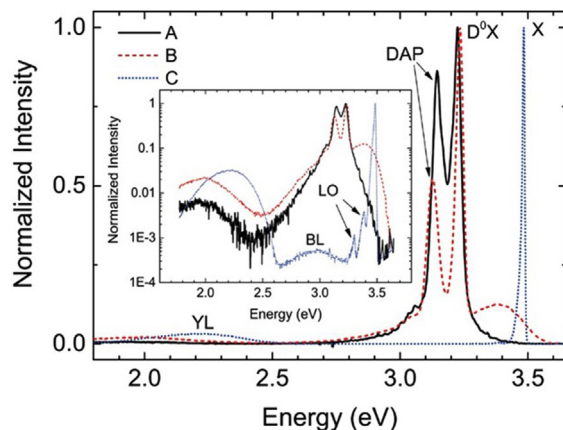
and cubic GaN; however, any BL band is hidden beneath a broad but weak band spanning from about 2.5–3.5 eV. This feature is even more prominent in the mixed cubic/hexagonal sample, reaching a peak at 3.4 eV and extending as far as 3.6 eV, i.e., higher than the bandgap of hexagonal GaN. This is the HEB discussed in Sec. IV B above that arises from the confinement of carriers between pairs of stacking faults, which, thus, form a QW structure; the large width of the HEB is due to the wide range of separations found between stacking fault pairs.[48]

## B. Quantum wells

There have only been a small number of reports on cubic QWs starting with that by Chichibu *et al.* in 2001, who described five QW stacks grown by MBE onto a bulk cubic GaN substrate.[75] They studied QWs containing 10% indium and with a range of QW widths from 0.6 to 10 nm. Later, Li *et al.*[76] investigated 6 QW stacks grown onto 3C-SiC substrates also via MBE and containing 16% indium with QW widths from 2 to 8 nm. Emission from cubic QWs across the visible, including in red, was demonstrated in 2016 by Orozco Hinostroza *et al.*,[77] who grew samples by MBE on MgO substrates. This was achieved by careful tuning of the growth conditions to enable the incorporation of up to 47% indium. Most recently, cubic QWs have been developed using MOCVD growth onto 3C-SiC substrates and have been shown to exhibit polarized emission[78] as well as being investigated for width-tunability and efficiency.[79]

### 1. Linewidth and tunability

Figure 11 shows an example of low-temperature emission spectra obtained from a set of MOCVD-grown samples each containing a stack of 5 QWs, with QW widths of 2.5, 5, and 7.5 nm; also shown is the emission from a single QW (SQW), also grown by MOCVD on 3C-SiC. Each spectrum is asymmetrical with a low energy tail, and the linewidths are very broad with FWHM values ranging between 280

**FIG. 10.** Low-temperature PL spectra obtained from epilayers that are >95% cubic GaN (a), and 50% cubic GaN (b), with the balance being hexagonal GaN; also shown for comparison are the spectra for an epilayer of pure hexagonal GaN (c). Peaks are indicated that are attributed to the recombination of free excitons (X); free excitons, with the recombination energy redshifted by the energy of one or two longitudinal optical (LO) phonons; donor bound excitons (D⁰X); donor–acceptor pairs (DAP); and the blue luminescence (BL) and yellow luminescence (YL) bands. The inset shows the same data on a logarithmic scale to enable the weaker features to be seen. Reproduced with permission from Church *et al.*, Phys. Status Solidi B **254**, 1600733 (2017). Copyright 2017 John Wiley and Sons.
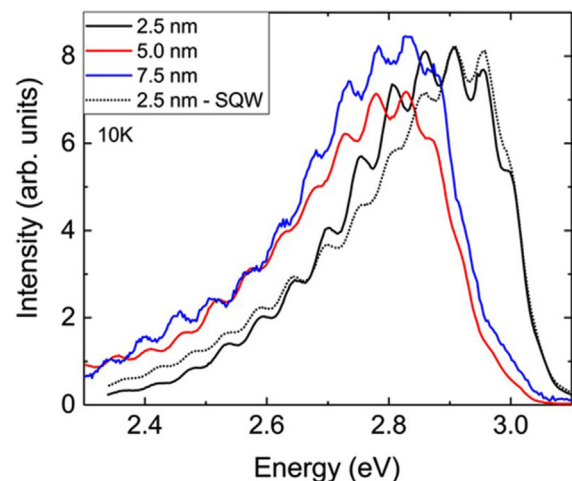
**FIG. 11.** Emission spectra for stacks of 5 QW with well widths of 2.5, 5, and 7.5 nm also shown is the spectrum for a single QW (SQW) of the width of 2.5 nm. Reproduced with permission from J. Appl. Phys. **129**, 175702 (2021). Copyright 2021 AIP Publishing.

and 300 meV. The spectra reported for samples grown by MBE on 3C-SiC[75] and other substrates[76,77] are in contrast more symmetrical but are of similar width. The width of the single QW spectrum shown in Fig. 11 is like that of the 5 QW stacks, indicating that it is due to inherent inhomogeneity within each well, rather than between wells. The asymmetry of the peaks obtained from the MOCVD-grown samples is attributed to the formation of quantum wire structures within the QW, which are produced due to the accumulation of In adjacent to the stacking faults.[80] These quantum wires emit a broad peak that overlaps with the lower energy side of the emission from the rest of the QWs; it is also highly polarized, an aspect which will be discussed further below. The emission peaks shown in Fig. 11 redshift with increasing well width, consistent with a reduction in the quantum confinement energy. Similar redshifts for greater QW width were also reported for the samples grown by MBE.[75,76]

### 2. Lifetime

Chichibu *et al.* found the recombination time to be approximately 300 ps at low temperature in their MBE-grown samples.[75] The recombination lifetime reported for the MOCVD samples was about twice as long and increased modestly for greater well widths, rising from 530 to 680 ps as well width is increased from 2.5 to 7.5 nm.[79] Nevertheless, these lifetimes are similar values to those found in non-polar m-plane hexagonal InGaN/GaN QWs[81] and consistent with recombination between co-localized electrons and holes, with the modest increase due to reducing confinement for greater well widths. In contrast, the lifetimes found in polar hexagonal QWs are much longer, typically tens of nanoseconds,[82] due to the spatial separation of the electron and holes and grow significantly longer as the well width increases. Thus, the radiative recombination rate in cubic QWs is much more competitive against non-radiative processes than for polar QWs.

### 3. Efficiency

Given that the development of cubic QWs is still ongoing, the efficiencies reported so far are likely not indicative of ultimate performance. Nevertheless, these initial studies provide useful insights into carrier dynamics in cubic QWs and into how QW number and thickness affect recombination efficiency. For MOCVD-grown samples, the emission efficiency at a low temperature of a SQW was observed to be about 70% of that of the 5 QW stacks, and this was attributed to a reduced carrier capture efficiency.[79] The efficiency of all the samples dropped as the temperature was raised. This was gradual until about 100 K and broadly independent of QW thickness and number and so was attributed to increasing recombination at defects as carriers become more mobile at elevated temperatures. However, the rate of this efficiency drop increased for temperatures greater than 100 K but was less pronounced for the 5 QW stacks compared to the SQW and for the thicker QWs. For the MBE-grown samples too, the emission intensity increased monotonically and significantly for greater QW width.[76] These observations are consistent with the onset of significant carrier loss from the QWs by thermionic emission and suggest that the emission efficiency can be improved by increasing the number of QWs in the stack and by increasing QW thickness, which, as noted above, does not bring the penalty of decreasing electron–hole

wave-function overlap and thereby the rate of radiative recombination, as is the case for polar hexagonal QWs.

Importantly, this increase in emission efficiency of the QWs with well width, rather than decreasing as is the case for polar hexagonal QWs, means that tuning cubic QWs to longer wavelengths by increasing the well thickness rather than by increasing indium content is a practical prospect, obviating the negative impact a higher indium fraction has on crystal quality. However, modeling, consistent with the results in Fig. 11, indicates that the tunability is weak for well widths above about 7.5 nm in thickness.[79] Even so, this range of QW thickness allows efficient emission to be extended to the green part of the spectrum without the loss of efficiency compared to cubic QWs emitting in the blue.

### 4. Droop

There are several reasons to expect that the onset of efficiency droop in cubic QWs will be at much higher rates of excitation, corresponding to higher drive currents in LEDs, than in polar QWs. First and foremost, among these reasons is, as discussed above, the much reduced recombination lifetime, which is typically about 0.5 ns in cubic QWs and can be tens or hundreds of nanoseconds in their polar analogs.[82] Since the carrier concentration resulting from a certain excitation rate is proportional to the lifetime, this should directly reduce the droop onset by about 2 orders of magnitude. A further reason is that larger well widths are practical for cubic QWs while they are not for polar ones, because of their negative impact on the wave-function overlap. Polar QWs are typically kept to about 3 nm, and so wider cubic QWs such as the 7.5 nm wide example shown in Fig. 11 will have a proportionally increased volume, reducing the carrier density for the same drive current. However, to date, there have been no reports that we are aware of on droop effects in cubic QWs, and so this area remains ripe for study.

### 5. Polarization

An unanticipated but useful property of cubic QWs is that their emission is linearly polarized to a significant degree, an effect attributed to indium accumulation adjacent to stacking faults where they intersect with the QWs.[80] This accumulation produces linear regions of reduced bandgap, forming quantum wires within the QW. Emission resulting from the recombination of carriers within these wires is preferentially polarized parallel to the wire. Moreover, it has been shown under the correct conditions[51] that the stacking faults are predominantly aligned in the $[1\bar{1}0]$ direction by the time they intersect with the QW so that light with a high degree of linear polarization (DOLP) is emitted from the QW overall. Figure 12 shows the polarization resolved emission spectra for 5 QW stacks for QW widths ranging from 2 to 8 nm; each sample was grown on 3C-SiC/Si (001) via MOCVD.[78] The DOLP for these samples was found to be broadly independent of QW width and reached 86% at low temperature, but remained as high as 75% at room temperature. As seen in Fig. 12, the dominant emission is polarized parallel to the $[1\bar{1}0]$ direction in the crystal and is centered at low energies than the weaker orthogonal emission. This is consistent with the polarized emission being from the quantum wires, which have a higher indium content than the surrounding QW and. hence, a lower bandgap, with the orthogonal emission coming mainly from the QW.
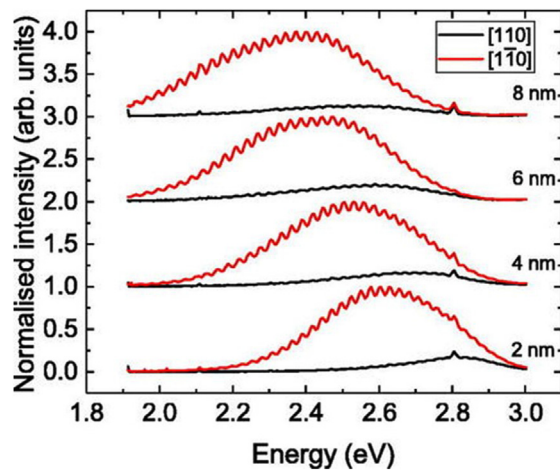
**FIG. 12.** Room temperature, polarization-resolved PL spectrum for cubic InGaN/GaN QW samples with QW widths ranging from 2 to 8 nm; each sample consists of 5 QWs grown by MOCVD. Excitation was by a continuous wave HeCd laser at a wavelength of 325 nm with an excitation power density of 10 W cm$^{-2}$. Reproduced with permission from Appl. Phys. Lett. **117**, 032103 (2020). Copyright 2020 AIP Publishing.

## VI. P-DOPING

The n- and p-type layers used in GaN LEDs are typically produced by doping with Si and Mg, respectively. Hexagonal GaN Mg-doped layers have been particularly thoroughly investigated over the last three decades since effective p-doping is more challenging than n-doping in hexagonal GaN.[25,74,83–88] An important issue is dopant passivation in MOCVD grown GaN due to the formation of an electrically inactive complex between Mg and hydrogen, which can be dissociated via post-growth thermal annealing.[25] In comparison to the numerous studies of p-doped hexagonal GaN, however, there have been relatively few reports on Mg-doped cubic GaN.[89–91] Most of these have been on MBE-grown samples, in which Mg-H complexes are less likely to form due to the absence of carrier gases. For MOCVD growth, which is more scalable and suitable for mass production, there have been very few reports on the effectiveness of annealing in reducing the passivation of Mg by hydrogen. In 2000, Xu et al.[92] published an initial study on the effectiveness of a rapid laser annealing technique. Much more recently, Dyer et al.[72] reported on the effects of conventional thermal annealing in a nitrogen atmosphere, concluding that it both increased the density of active Mg dopants, thus enhancing hole conductivity and reduced non-radiative recombination.

## VII. DEVICES AND APPLICATIONS

Based on the fundamental properties of cubic GaN described above there is clear potential for enhanced device performance, particularly for optical devices such as LEDs. However, to date, there have been relatively few attempts to make full devices in this promising material. Yang et al.[93] reported a blue-emitting LED grown on a GaAs substrate and based on a simple p–n junction without QWs. This device showed electroluminescence at around 430 nm with a linear increase in peak intensity between drive current densities of 50–350 A cm$^{-2}$ and a turn-on voltage of 6 V. A similar p–n junction device was demonstrated by Gamez-Cuatzin et al.[94] grown on a 3C-SiC/Si substrate. In this case, green (2.5 eV) emission was seen at low drive currents (32 mA), which shifted to blue (3.1 eV) at higher drive currents (70 mA). In both these examples, no attempt was made to quantify the efficiency of the device and the authors ascribe the emission to defect mediated recombination. As et al.[95] have also demonstrated a cubic GaN p–n junction LED on GaAs. In this device, band edge electroluminescence was seen at 3.2 eV again with a linear increase in intensity with drive current. Based on a comparison of PL and electroluminescence intensities the authors estimate the efficiency of this device at around $1 \times 10^{-3}$. Beyond these examples of devices demonstrated around the year 2000, there has been very little work on cubic GaN devices until more recently. Stark et al.[14] have demonstrated cubic GaN QW LEDs structures grown on patterned Si substrates. In this case, the LEDs were formed in approximately 500 nm wide stripes of cubic GaN confined within V-grooves in the Si substrate. These devices showed emissions between 487 and 516 nm with an estimated external quantum efficiency of $3 \times 10^{-5}$.

Building on the growth and characterization studies described in this manuscript, our work has also been extended by a spin-out company, Kubos Semiconductors Ltd, to examine the development of cubic-GaN based LEDs. This has delivered full MQW LED structures emitting across the green and amber region of the optical spectrum. Some examples of such cubic GaN LEDs are shown in Fig. 13. For device (a), the peak emission occurs at 530 nm and device (b) at 600 nm. These devices clearly demonstrate promising progress in the development of cubic GaN LEDs, and the work is under progress to further improve the efficiency and operability of these devices.

To the best of our knowledge, only two attempts have been made to demonstrate electronic devices in cubic GaN. The first of these was a Schottky diode using a 30 nm Al$_{0.3}$GaN$_{0.7}$/GaN heterostructure with a Ni metal contact. Rectifying behavior and a breakdown voltage of 80 V at a doping level of $1.8 \times 10^{17}$ cm$^{-2}$ were demonstrated.[96] The second was also a Schottky diode device, which in this case was
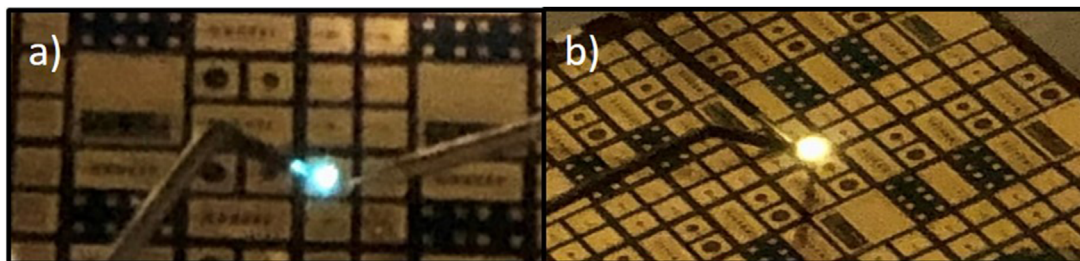


**FIG. 13.** Images of biased cubic GaN LEDs. Device (a) has a peak emission at 530 nm, and device (b) has a peak emission at 600 nm.

designed to be used as an x-ray detector.[97] The device structures produced consisted of 6 or 0.5 $\mu$m of Si-doped cubic GaN layers grown by MBE on GaAs substrates. The Schottky contacts were 20 nm Ni/ 40 nm Au and the dark current, capacitance, and detection efficiency of the devices were studied for various areas and epilayer thicknesses.

The very promising properties of cubic GaN mean that it could offer improved performance in a wide range of applications. Clearly, one of the key drivers for pursuing cubic GaN devices is the generation of more efficient long wavelength LEDs. These would have clear benefits in solid state lighting and would be a key enabler for a switch from phosphor converted white light emitters to multi-color LEDs. Due to the inherent losses involved in converting blue light emitted from an LED to yellow light using a phosphor, the practical limit for luminous efficacy of such white light sources is about 255 lm W$^{-1}$. For white light based on efficient multi-color LEDs, a theoretical luminous efficacy of 325 lm W$^{-1}$ could be achieved. Therefore, the U.S. DoE in its 2019 report on "Lighting R&D opportunities" highlights the development of higher efficiency green and amber LEDs as a key requirement to deliver the energy saving potential of solid-state lighting.[1] Lighting solutions based on efficient multi-color LEDs also offer the opportunity to tune the color spectrum of the lit environment. This would allow, for example, luminaires that mimic natural daylight, which has been shown to have a significant impact on children's concentration at school, productivity in the workplace, and people's health.[1]

Another technology area where the poor efficiency of long wavelength LEDs is a significant roadblock is micro-LED displays. These offer significant reductions in energy usage, higher intensity for use in bright environments, and better contrast ratios and are being developed by all major display manufacturers and integrators. In this case, it is not only the drop-off in efficiency at longer wavelengths known as the "green gap," but also a reduction in efficiency associated with reduced device area, which is problematic. For virtual reality (VR) and augmented reality (AR) applications, individual LED sizes below 5 $\mu$m are needed in order to achieve the required display resolution. It has been found that for such strongly scaled devices, the efficiency of InGaAlP LEDs, normally used for red emission, collapses to only a few percent for devices below about 30 $\mu$m.[98] Therefore, there is significant interest in extending the use of GaN LEDs into red as nitride-based LEDs have been shown to be more robust to devise scaling. Blue GaN LEDs have been demonstrating efficiencies around 40% down to 10 $\mu$m in size.[99] As discussed above, cubic GaN LEDs are expected to deliver higher efficiencies out to longer wavelengths and if the improved scalability of conventional nitride LEDs is maintained, they could offer a solution for both green and red pixels in micro-LED displays. It is also worth noting that for larger displays such as computer monitors and TVs, although the resolution requirements do not dictate the use of such small LED die, cost considerations to allow the use of directly illuminated displays do require very small LED sizes in order to meet the price requirements in mass consumer markets.

The significantly reduced carrier lifetimes offered by cubic GaN due to the removal of the internal electric field across QWs provide an opportunity not only to improve device efficiencies but also (for correctly designed devices) to create LEDs that are capable of being switched on and off very quickly. This high switching speed can be utilized in a range of communications applications. These include LiFi, the light equivalent of WiFi, which is being developed to address the very crowded use of the radio frequency spectrum for free-space data transmission and chip-to-chip and server-to-server communication. In both cases, the current technologies are reaching their capacity limits, and therefore, if the current growth in data usage is to be maintained innovative solutions are mandated.

Beyond LEDs, there is also interest in developing lasers based on cubic GaN. For similar reasons to those discussed for LEDs, the efficiency of nitride-based lasers is also impacted by the QCSE, and in principle, cubic GaN offers a route to improve such devices although based on experience with hexagonal GaN, this will place stringent requirements on defect density reduction. Efficient long wavelength lasers have applications in pico-projector technologies where they could be used to project images onto surfaces from mobile devices removing the need for built-in displays. Increased efficiency is also desirable in large area projector systems such as those used in cinemas as the heat generated by conventional light sources often adds significantly to system complexity and cost.

## VIII. CONCLUSIONS AND OUTLOOK

The renewed interest in zinc-blende GaN stems from the recognition that its cubic crystal structure could help to address some of the most important and persistent challenges with the performance of GaN-based LEDs, such as their lower efficiency at high drive currents and when emitting in the green and amber parts of the visible spectrum. The greater symmetry of the cubic phase results in InGaN/GaN QWs free of the polarization fields that tend to suppress the rate of radiative recombination in conventional wurtzite quantum wells grown along the c-axis, an effect which is exacerbated for greater well thicknesses and for the higher indium contents needed to achieve longer wavelength emission. The reduced recombination lifetime in cubic QWs compared to their hexagonal analogs also means that it should be possible to modulate them at a much higher rate, promising enhanced data rates in LiFi and other visible light communications systems. Furthermore, considerable progress has been made in growing this thermodynamically unstable phase so that phase-pure samples are now available grown by the commercially relevant MOCVD method.

Recent progress in the performance of cubic InGaN/GaN QWs and LEDs is promising, with emission now demonstrated that can be redshifted by increasing the QW thickness without the loss of efficiency. The discovery that the emission from cubic QWs can also be linearly polarized to a significant degree was unexpected and opened further avenues for exploitation, such as in display technologies. However, the work reported to date on the properties and performance of these QWs still remains limited. Further studies are required to optimize the number and width of QWs for high efficiency and to understand the causes underlying the broad emission linewidth. There have also not yet been any reports on the performance of cubic QWs at high excitation rates, even though their reduced recombination lifetimes compared to hexagonal QWs will reduce the carrier density resulting from a certain drive current density, significantly ameliorating the effects of efficiency droop.

The scene is, thus, set for cubic GaN to have a significant impact on a number of important applications in the coming few years, with high brightness applications such as vehicle headlights and fast LiFi in particular, likely to most benefit from the properties resulting from the enhanced symmetry of its crystal structure.

## AUTHOR DECLARATIONS
### Conflict of Interest

D. J. Wallis is a director of and owns stock in, Kubos Semiconductors, Ltd. D. J. Wallis has patent No. PCT/EP2018/058250 granted in the U.S. and Singapore and pending elsewhere. R. O. Oliver, D. J. Binks, P. Dawson, and D. J. Wallis have patent No. PCT/EP2020/077339 pending.

### Author Contributions

**D. J. Binks:** Writing – original draft (equal); Writing – review and editing (equal). **P. Dawson:** Writing – original draft (equal). **R. A. Oliver:** Writing – original draft (equal); Writing – review and editing (equal). **D. J. Wallis:** Writing – original draft (equal); Writing – review and editing (equal).

### DATA AVAILABILITY

The previously unreported data shown in Figs. 1 and 5 are openly available from the 'Figshare' repository at http://doi.org/10.48420/19614471.

## REFERENCES

[1] M. Pattison, M. Hansen, N. Bardsley, C. Elliiot, K. Lee, L. Pattison, and J. Tsao, "Lighting R&D opportunities" Report No. DOE/EE-2008 8189 (U.S. Department of Energy, Office of Energy Efficiency and Renewable Energy, 2019).

[2] M. Auf der Maur, A. Pecchia, G. Penazzi, W. Rodrigues, and A. Di Carlo, Phys. Rev. Lett. **116**, 027401 (2016).

[3] G. Verzellesi, D. Saguatti, M. Meneghini, F. Bertazzi, M. Goano, G. Meneghesso, and E. Zanoni, J. Appl. Phys. **114**, 071101 (2013).

[4] M. Leszczynski, H. Teisseyre, T. Suski, I. Grzegory, M. Bockowski, J. Jun, S. Porowski, K. Pakula, J. M. Baranowski, C. T. Foxon, and T. S. Cheng, Appl. Phys. Lett. **69**, 73 (1996).

[5] J. W. Fan, M. F. Li, T. C. Chong, and J. B. Xia, J. Appl. Phys. **79**, 188 (1996).

[6] C. A. Hernández-Gutiérre, Y. L. Casallas-Moreno, V.-T. Rangel-Kuoppa, D. Cardona, Y. Hu, Y. Kudriatsev, M. A. Zambrano-Serrano, S. Gallardo-Hernandez, and M. Lopez-Lopez, Sci. Rep. **10**, 16858 (2020).

[7] See www.ioffe.ru for bandgap data.

[8] F. Schwierz, Solid-State Electron. **49**, 889 (2005).

[9] D. J. As, A. Richter, J. Busch, B. Schöttker, M. Lübbers, J. Mimkes, D. Schikora, K. Lischka, W. Kriegseis, W. Burkhardt, and B. K. Meyer, MRS Internet J. Nitride Semicond. Res. **5**, 308 (2000).

[10] M. Horita, S. Takashima, R. Tanaka, H. Matsuyama, K. Ueno, M. Edo, T. Takahashi, M. Shimizu, and J. Suda, Jpn. J. Appl. Phys., Part 1 **56**, 031001 (2017).

[11] A. F. Wright and J. S. Nelson, Phys. Rev. B **50**, 2159 (1994).

[12] A. Nakadaira and H. Tanaka, J. Electron. Mater. **26**, 320 (1997).

[13] S. V. Novikov, N. Zainal, A. V. Akimov, C. R. Staddon, A. J. Kent, and C. T. Foxon, J. Vac. Sci. Technol. B **28**, C3B1 (2010).

[14] C. J. M. Stark, T. Detchprohm, S. C. Lee, Y.-B. Jiang, S. R. J. Brueck, and C. Wetzel, Appl. Phys. Lett. **103**, 232107 (2013).

[15] C. Bayram, J. A. Ott, K.-T. Shiu, C.-W. Cheng, Y. Zhu, J. Kim, M. Razeghi, and D. K. Sadana, Adv. Funct. Mater. **24**, 4492 (2014).

[16] A. Yamada, T. Maruyama, and K. Akimoto, J. Cryst. Growth **189–190**, 401 (1998).

[17] J. Wu, H. Yaguchi, B. P. Zhang, Y. Segawa, K. Onabe, and Y. Shiraki, Phys. Status Solidi A **180**, 403 (2000).

[18] C. H. Wei, Z. Y. Xie, L. Y. Li, Q. M. Yu, and J. H. Edgar, J. Electron. Mater. **29**, 317 (2000).

[19] S. V. Novikov, A. J. Kent, and C. T. Foxon, Prog. Cryst. Growth Charact. Mater. **63**, 25 (2017).

[20] M. Frentrup, L. Y. Lee, S. L. Sahonta, M. J. Kappers, F. Massabuau, P. Gupta et al., J. Phys. D: Appl. Phys. **50**, 433002 (2017).

[21] D. Zhu, D. J. Wallis, and C. J. Humphreys, Rep. Prog. Phys. **76**, 106501 (2013).

[22] L. Y. Lee, M. Frentrup, M. J. Kappers, R. A. Oliver, C. J. Humphreys, and D. J. Wallis, J. Appl. Phys. **124**, 105302 (2018).

[23] Y. X. Feng, X. L. Yang, Z. H. Zhang, D. Kang, J. Zhang, K. H. Liu, X. Z. Li, J. F. Shen, F. Liu, T. Wang, P. F. Ji, F. J. Xu, N. Tang, T. J. Yu, X. Q. Wang, D. P. Yu, W. K. Ge, and B. Shen, Adv. Funct. Mater. **29**, 1905056 (2019).

[24] H. Tang and J. B. Webb, Appl. Phys. Lett. **74**, 2373 (1999).

[25] S. Nakamura, N. Iwasa, M. Senoh, and T. Mukai, Jpn. J. Appl. Phys., Part 1 **31**, 1258 (1992).

[26] D. Wang, Y. Hiroyama, M. Tamura, and M. Ichikawa, Appl. Phys. Lett. **76**, 1683 (2000).

[27] A. Trampert, 0. Brandt, H. Yang, and K. H. Ploog, Appl. Phys. Lett. **70**, 583 (1997).

[28] H. Yang, O. Brandt, and K. Ploog, Phys. Status Solidi B **194**, 109 (1996).

[29] T. Ohachi, T. Kikuchi, A. Somintac, S. Yamaguchi, T. Yasuda, and M. Wada, Phys. Status Solidi C **3**(6), 1404–1407 (2006).

[30] L. C. Jenkins, T. S. Cheng, C. T. Foxon, S. E. Hooper, J. W. Orton, S. V. Novikov, and V. V. Tret'yakov, J. Vac. Sci. Technol. B **13**, 1585 (1995).

[31] S. V. Novikov, N. M. Stanton, R. P. Campion, R. D. Morris, H. L. Geen, C. T. Foxon, and A. J. Kent, Semicond. Sci. Technol. **23**, 015018 (2008).

[32] M. Mizuta, S. Fujieda, Y. Matsumoto, and T. Kawamura, Jpn. J. Appl. Phys., Part 2 **25**, L945–L948 (1986).

[33] G. Parish, S. Keller, S. P. Denbaars, and U. K. Mishra, J. Elec. Mat. **29**, 15 (2000).

[34] H. Amano, I. Akasaki, K. Hiramatsu, N. Koide, and N. Sawaki, Thin Solid Films **163**, 415 (1988).

[35] H. Vilchis, V. M. Sanchez-R, and A. Escobosa, in Proceedings of the 8th International Caribbean Conference on Devices, Circuits and Systems (IEEE, 2012), pp. 1–3.

[36] J. Wu, H. Yaguchi, K. Onabe, Y. Shiraki, and R. Ito, Jpn. J. Appl. Phys., Part 1 **37**, 1440 (1998).

[37] J. Camassel, P. Vicente, N. Planes, J. Allègre, J. Pankove, and F. Namavar, Phys. Status Solidi B **216**, 253 (1999).

[38] J. Wu, H. Yaguchi, K. Onabe, and R. Ito, Appl. Phys. Lett. **71**(15), 2067 (1997).

[39] E. B. Yakimov, J. Alloys Compd. **627**, 344 (2015).

[40] J. F. Muth, J. H. Lee, I. K. Shmagin, R. M. Kolbas, H. C. Casey, Jr., B. P. Keller, U. K. Mishra, and S. P. DenBaars, Appl. Phys. Lett. **71**, 2572 (1997).

[41] U. Haboeck, H. Siegle, A. Hoffmann, and C. Thomsen, Phys. Status Solidi C **0**(6), 1710–1731 (2003).

[42] J. W. Roberts, J. C. Jarman, D. N. Johnstone, P. A. Midgley, P. R. Chalker, R. A. Oliver, and F. C.-P. Massabuau, J. Cryst. Growth **487**, 23 (2018).

[43] Y. J. Sun, O. Brandt, U. Jahn, T. Y. Liu, A. Trampert, S. Cronenberg, S. Dhar, and K. H. Ploog, J. Appl. Phys. **92**, 5714 (2002).

[44] P. Corfdir and P. Lefebvre, J. Appl. Phys. **112**, 053512 (2012).

[45] C. Chèze, L. Geelhaar, B. Jenichen, and H. Riechert, Appl. Phys. Lett. **97**, 153105 (2010).

[46] G. Jacopin, L. Rigutti, L. Largeau, F. Fortuna, F. Furtmayr, F. H. Julien, M. Eickhoff, and M. Tchernycheva, J. Appl. Phys. **110**, 064313 (2011).

[47] M. Murayama and T. Nakayama, Phys. Rev. B **49**, 4710 (1994).

[48]S. A. Church, S. Hammersley, P. W. Mitchell, M. J. Kappers, L. Y. Lee, F. Massabuau, S. L. Sahonta, M. Frentrup, L. J. Shaw, D. J. Wallis, C. J. Humphreys, R. A. Oliver, D. J. Binks, and P. Dawson, J. Appl. Phys. **123**, 185705 (2018).

[49]D. S. P. Tanner, J. M. McMahon, and S. Schulz, Phys. Rev. Appl. **10**, 034027 (2018).

[50]X. M. Shen, Y. Fu, G. Feng, B. S. Zhang, Z. H. Feng, Y. T. Wang, and H. Yang, J. Cryst. Growth **246**, 69 (2002).

[51]L. Y. Lee, M. Frentrup, P. Vacek, M. J. Kappers1, D. J. Wallis, and R. A. Oliver, J. Appl. Phys. **125**, 105303 (2019).

[52]C. Stampfl and C. G. Van de Walle, Phys. Rev. B **57**(24), R15052 (1998).

[53]I. Vurgaftman and J. R. Meyer, J. Appl. Phys. **94**(6), 3675 (2003).

[54]F. Bernardini and V. Fiorentini, Phys. Status Solidi B **216**, 391 (1999).

[55]P. Vacek, M. Frentrup, L. Y. Lee, F. C.-P. Massabuau, M. J. Kappers, D. J. Wallis, R. Gröger, and R. A. Oliver, J. Appl. Phys. **129**, 155306 (2021).

[56]M. A. Reshchikov and H. Morkoç, J. Appl. Phys. **97**(6), 061301 (2005).

[57]M. Feneberg, M. Röppischer, C. Cobet, N. Esser, J. Schörmann, T. Schupp, D. J. As, F. Hörich, J. Bläsing, A. Krost, and R. Goldhahn, Phys. Rev. B **85**, 155207 (2012).

[58]G. Ramirez-Flores, H. Navarro-Contreras, A. Lastras-Martinez, R. C. Powell, and J. E. Greene, Phys. Rev. B **50**, 8433 (1994).

[59]D. Xu, H. Yang, J. B. Li, D. G. Zhao, S. F. Li, S. M. Zhuang, and R. H. Wu, Appl. Phys. Lett. **76**, 3025 (2000).

[60]H. Yaguchi, J. Wu, B. Zhang, Y. Segawa, H. Nagasawa, K. Onabe, and Y. Shiraki, J. Cryst. Growth **195**, 323 (1998).

[61]J. Menniger, U. Jahn, O. Brandt, H. Yang, and K. Ploog, Phys. Rev. B **53**, 1881 (1996).

[62]U. Strauß, H. Tews, H. Riecher, R. Averbeck, M. Schienle, B. Jobst, D. Volm, T. Streibl, B. K. Meyer, and W. W. Ruhle, Semicond. Sci. Technol. **12**, 637 (1997).

[63]A. V. Andrianov, D. E. Lacklison, J. W. Orton, T. S. Cheng, C. T. Foxon, K. P. O'Donnell, and J. F. H. Nicholls, Semicond. Sci. Technol. **12**, 59 (1197).

[64]D. J. As, F. Schmilgus, C. Wang, B. Schöttker, D. Schikora, and K. Lischka, Appl. Phys. Lett. **70**, 1311 (1997).

[65]Z. X. Liu, A. R. Goñi, and K. Syassen, J. Appl. Phys. **86**, 929 (1999).

[66]B. Daudin, G. Feuillet, J. Hűbner, Y. Samson, F. Widmann, A. Philippe, C. Bru-Chevallier, G. Guillot, E. Bustarret, G. Bentoumi, and A. Deneuville, J. Appl. Phys. **84**, 2295 (1998).

[67]U. Köhler, M. Lübbers, J. Mimkes, and D. J. As, Phys. Status Solidi B **308–310**, 126 (2001).

[68]D. J. As, U. Köhler, M. Lübbers, J. Mimkes, and K. Lischka, Phys. Status Solidi **188**, 699 (2001).

[69]R. E. L. Powell, S. V. Novikov, C. T. Foxon, A. V. Akimov, and A. J. Kent, Phys. Status Solidi C **11**, 385 (2014).

[70]D. J. As, T. Simonsmeier, B. Schöttker, T. Frey, D. Schikora, W. Kriegseis, W. Burkhardt, and B. K. Meyer, Appl. Phys. Lett. **73**, 1835 (1998).

[71]M. A. Reshchikov, J. Appl. Phys. **127**, 055701 (2020).

[72]D. Dyer, S. A. Church, M. Jain, M. J. Kappers, M. Frentrup, D. J. Wallis, R. A. Oliver, and D. J. Binks, J. Appl. Phys. **130**, 085705 (2021).

[73]F. Shahedipour and B. W. Wessels, Appl. Phys. Lett. **76**, 3011 (2000).

[74]Z. Q. Li, H. Chen, H. F. Liu, L. Wan, M. H. Zhang, Q. Huang, J. M. Zhou, N. Yang, K. Tao, Y. J. Han, and Y. Luo, Appl. Phys. Lett. **76**, 3765 (2000).

[75]S. F. Chichibu, M. Sugiyama, T. Onuma, T. Kitamura, H. Nakanishi, T. Kuroda, A. Tackeuchi, T. Sota, Y. Ishida, and H. Okumura, Appl. Phys. Lett. **79**(26), 4319 (2001).

[76]S. Li, J. S. Schörmann, D. J. As, and K. Lischka, Appl. Phys. Lett. **90**(7), 071903 (2007).

[77]I. Orozco Hinostroza, M. Avalos-Borja, V. Compean Garcia, C. C. Zamora, A. Rodriguez, E. Lopez Luna, and M. Vidal, J. Cryst. Growth **435**, 110 (2016).

[78]S. A. Church, B. Ding, P. W. Mitchell, M. J. Kappers, M. Frentrup, G. Kusch, S. M. Fairclough, D. J. Wallis, R. A. Oliver, and D. J. Binks, Appl. Phys. Lett. **117**, 032103 (2020).

[79]S. A. Church, M. Quinn, K. Cooley-Greene, B. Ding, A. Gundimeda, M. J. Kappers, M. Frentrup, D. J. Wallis, R. A. Oliver, and D. J. Binks, J. Appl. Phys. **129**, 175702 (2021).

[80]B. Ding, M. Frentrup, S. M. Fairclough, M. J. Kappers, M. Jain, A. Kovács, D. J. Wallis, and R. A. Oliver, J. Appl. Phys. **128**, 145703 (2020).

[81]P. Dawson, S. Schulz, R. A. Oliver, M. J. Kappers, and C. J. Humphreys, J. Appl. Phys. **119**, 181505 (2016).

[82]A. David and M. J. Grundmann, Appl. Phys. Lett. **97**, 033501 (2010).

[83]U. Kaufmann, M. Kunzer, M. Maier, H. Obloh, A. Ramakrishnan, B. Santic, and P. Schlotter, Appl. Phys. Lett. **72**, 1326 (1998).

[84]A. Castiglia, J.-F. Carlin, and N. Grandjean, Appl. Phys. Lett. **98**, 213505 (2011).

[85]M. Sumiya, K. Fukuda, S. Takashima, S. Ueda, T. Onuma, T. Yamaguchi, T. Honda, and A. Uedono, J. Cryst. Growth **511**, 15 (2019).

[86]M. A. Reshchikov, P. Ghimire, and D. O. Demchenko, Phys. Rev. B **97**, 205204 (2018).

[87]S. F. Chichibu, K. Shima, K. Kojima, S. Takashima, M. Edo, K. Ueno, S. Ishibashi, and A. Uedono, Appl. Phys. Lett. **112**, 211901 (2018).

[88]A. Klump, M. P. Hoffmann, F. Kaess, J. Tweedie, P. Reddy, R. Kirste, Z. Sitar, and R. Collazo, J. Appl. Phys. **127**, 045702 (2020).

[89]E. Martinez-Guerrero, B. Daudin, G. Feuillet, H. Mariette, Y. Genuist, S. Fanget, A. Philippe, C. Dubois, C. Bru-Chevallier, G. Guillot, P. Aboughe Nze, T. Chassagne, Y. Monteil, H. Gamez-Cuatzin, and J. Tardy, Mater. Sci. Eng. B **82**, 59 (2001).

[90]D. Xu, H. Yang, D. G. Zhao, S. F. Li, and R. H. Wu, J. Appl. Phys. **87**, 2064 (2000).

[91]D. J. As, Phys. Status Solidi B **210**, 445 (1998).

[92]D. Xu, H. Yang, S. Li, D. Zhao, H. Ge, and R. Wu, J. Cryst. Growth **209**, 203 (2000).

[93]H. Yang, L. X. Zheng, J. B. Li, X. J. Wang, D. P. Xu, Y. T. Wang, and X. W. Hu, Appl. Phys. Lett. **74**, 2498 (1999).

[94]H. Gamez-Cuatzin, J. Tardy, P. Rojo-Romeo, A. Philippe, C. Bru-Chevallier, A. Souifi, G. Guillot, E. Martinez-Guerrero, G. Feuillet, B. Daudin, P. Aboughé-Nzé, and Y. Monteil, Phys. Status Solidi A **176**, 131 (1999).

[95]D. J. As, A. Richter, J. Busch, M. Lübbers, J. Mimkes, and K. Lischka, Appl. Phys. Lett. **76**, 13 (2000).

[96]M. Abe, H. Nagasawa, S. Potthasr, J. Fernandez, J. Schörmann, D. J. As, and K. Lischka, IEICE Trans. Electron. **E89-C**(7), 1057 (2006).

[97]T. Gohil, J. Whale, G. Lioliou, S. V. Novikov, C. T. Foxon, A. J. Kent, and A. M. Barnett, Sci. Rep. **6**, 29535 (2016).

[98]J.-T. Oh, S.-Y. Lee, Y.-T. Moon, J. H. Moon, S. Park, K. Y. Hong, K. Y. Song, C. Oh, J.-I. Shim, H.-H. Jeong, J.-O. Song, H. Amano, and T.-Y. Seong, Opt. Express **26**, 11194 (2019).

[99]D. Hwang, A. Mughal, C. D. Pynn, S. Nakamura, and S. P. DenBaars, Appl. Phys. Express **10**, 032101 (2017).

[100]D. J. Wallis and M. J. Kappers (2022). "Peak photoluminescence wavelengths for quantum well thicknesses between 2 nm and 10nm, and a comparison of the photoluminescence spectra from epilayers of wurtzite and zincblende GaN," Figshare. http://doi.org/10.48420/19614471